Electronic Supplementary Material (ESI) for Physical Chemistry Chemical Physics.


# Supplementary Material: Machine learning search for stable binary Sn alloys with Na, Ca, Cu, Pd, and Ag

Aidan Thorn, Daviti Gochitashvili, Saba Kharabadze, and Aleksey N. Kolmogorov
*Department of Physics, Applied Physics and Astronomy,*
*Binghamton University, State University of New York,*
*PO Box 6000, Binghamton, New York 13902-6000, USA*
(Dated: June 16, 2023)

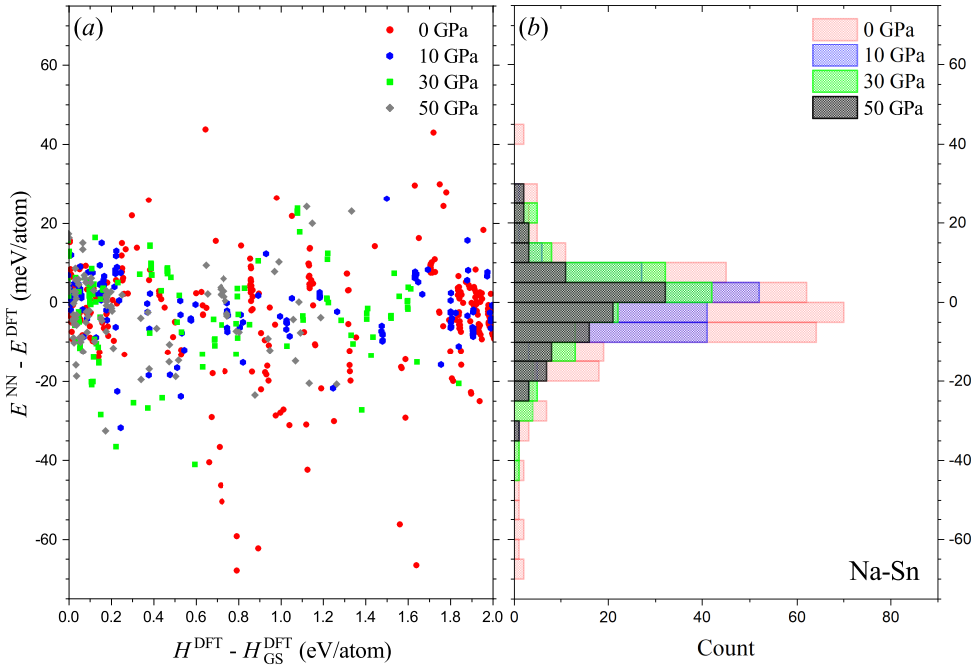


Supplementary Figure 1. Performance of the developed NN model against the reference DFT approximation for Na-Sn phases at 0-50 GPa. (a) NN energy errors vs relative enthalpies for testing set structures fully optimized with the DFT. The relative enthalpies were calculated with respect to the most stable phase at each composition and pressure. (b) The histogram of the NN energy errors.

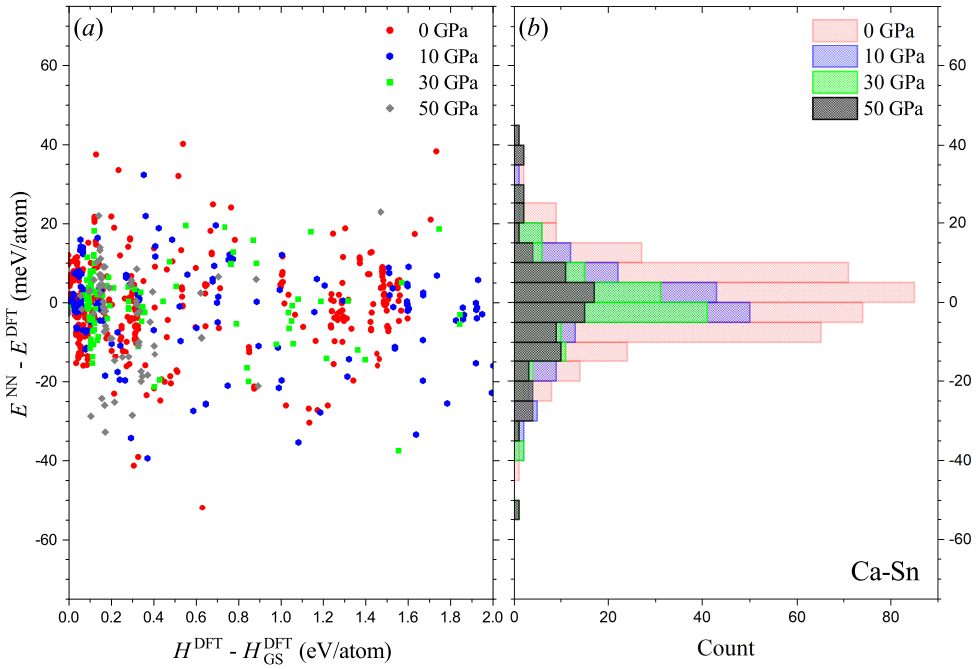


Supplementary Figure 2. Performance of the developed NN model against the reference DFT approximation for Ca-Sn phases at 0-50 GPa. (a) NN energy errors vs relative enthalpies for testing set structures fully optimized with the DFT. The relative enthalpies were calculated with respect to the most stable phase at each composition and pressure. (b) The histogram of the NN energy errors.

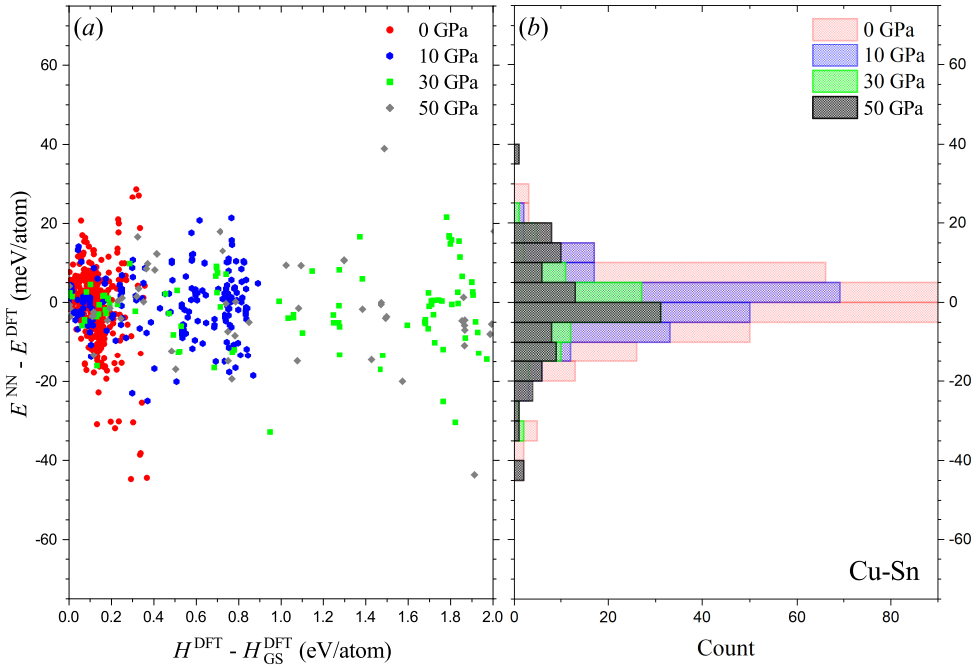


Supplementary Figure 3. Performance of the developed NN model against the reference DFT approximation for Cu-Sn phases at 0-50 GPa. (a) NN energy errors vs relative enthalpies for testing set structures fully optimized with the DFT. The relative enthalpies were calculated with respect to the most stable phase at each composition and pressure. (b) The histogram of the NN energy errors.

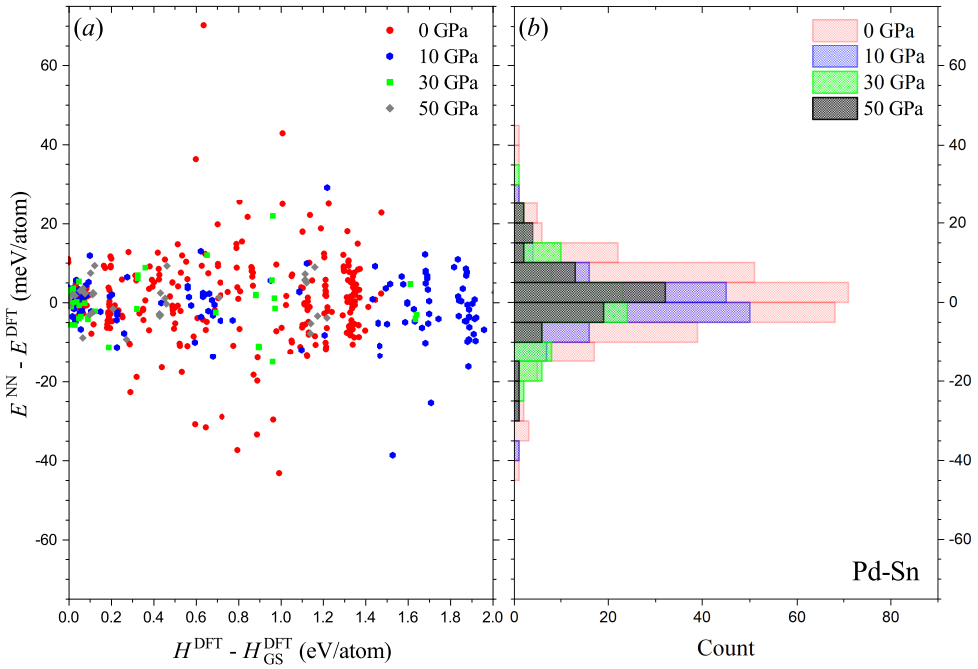


Supplementary Figure 4. Performance of the developed NN model against the reference DFT approximation for Pd-Sn phases at 0-50 GPa. (a) NN energy errors vs relative enthalpies for testing set structures fully optimized with the DFT. The relative enthalpies were calculated with respect to the most stable phase at each composition and pressure. (b) The histogram of the NN energy errors.

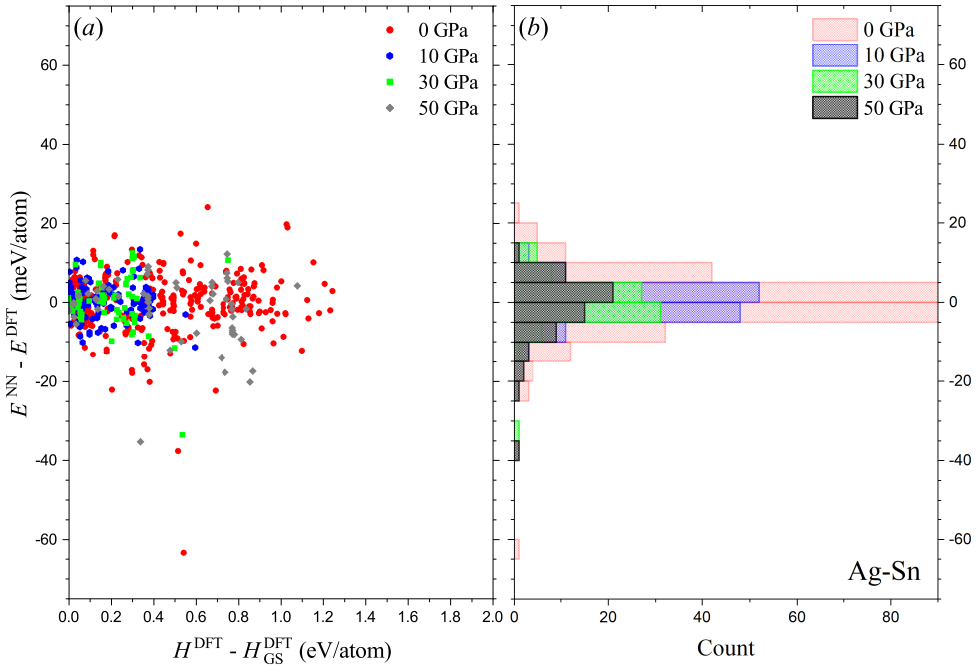


Supplementary Figure 5. Performance of the developed NN model against the reference DFT approximation for Ag-Sn phases at 0-50 GPa. (a) NN energy errors vs relative enthalpies for testing set structures fully optimized with the DFT. The relative enthalpies were calculated with respect to the most stable phase at each composition and pressure. (b) The histogram of the NN energy errors.

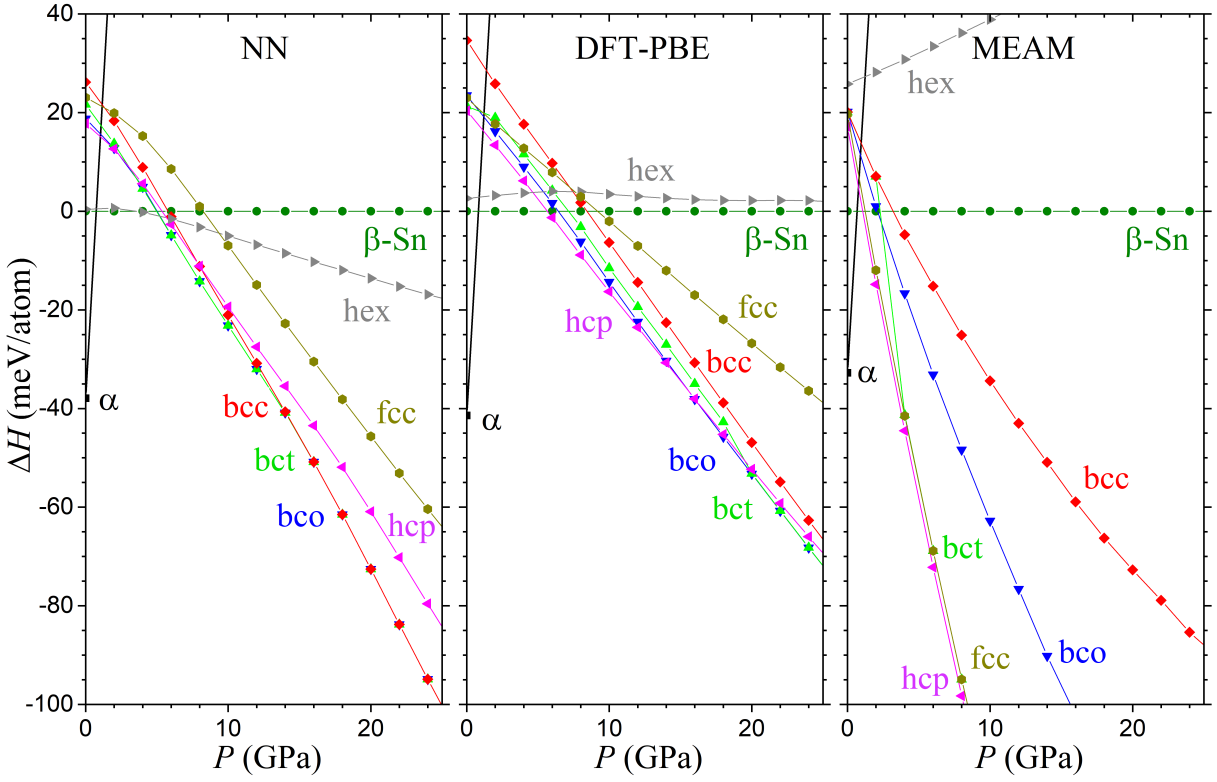


Supplementary Figure 6. Relative enthalpies for select Sn phases evaluated with our neural network (NN) model, the reference DFT approximation, and the modified embedded atom model (MEAM) developed in Ref. Ko, W.-S., Kim, D.-H., Kwon, Y.-J. & Lee, M., *Metals* **8**, 900 (2018).

| Phase | Relative to | PBE | LDA | SCAN |
|---|---|---|---|---|
| mP20-$Na_4Sn$* | hcp-Na ↔ cI76-$Na_{15}Sn_4$ | 0.4 | 2.9 | 0.8 |
| hR21-$Na_5Sn_2$ | cI76-$Na_{15}Sn_4$ ↔ hP60-$Na_7Sn_3$ | 4.4 | 1.1 | 1.8 |
| oS52-$Na_9Sn_4$ | hP60-$Na_7Sn_3$ ↔ tI64-NaSn | 4.8 | 5.8 | 8.2 |
| mS24-$Na_2Sn$† | hP60-$Na_7Sn_3$ ↔ tI64-NaSn | 1.2 | -0.2 | -3.1 |
| mP78-$Na_5Sn_8$ | tI64-NaSn ↔ aP76-$Na_7Sn_{12}$ | 1.8 | -0.1 | 1.5 |
| aP76-$Na_7Sn_{12}$ | mP78-$Na_5Sn_8$ ↔ mS48-$NaSn_2$ | -3.4 | -2.3 | -6.5 |
| hP3-$NaSn_2$ | mS48-$NaSn_2$ | 2.0 | -17.2 | -10.4 |
| hP3-$NaSn_2$ | aP76-$Na_7Sn_{12}$ ↔ $\alpha$-Sn | 4.7 | -17.4 | -2.2 |
| hP6-$NaSn_2$* | mS48-$NaSn_2$ | 0.2 | -10.2 | -11.4 |
| hP6-$NaSn_2$* | aP76-$Na_7Sn_{12}$ ↔ $\alpha$-Sn | 2.8 | -10.4 | -3.2 |
| mS48-$NaSn_2$ | aP76-$Na_7Sn_{12}$ ↔ $\alpha$-Sn | 2.6 | -0.2 | 8.3 |
| oS288-$Na_5Sn_{13}$ | mS48-$NaSn_2$ ↔ $\alpha$-Sn | 20.5 | - | - |
| oS288-$Na_5Sn_{13}$ | aP76-$Na_7Sn_{12}$ ↔ $\alpha$-Sn | 22.7 | - | - |
| oP12-$NaSn_3$ | mS48-$NaSn_2$ ↔ $\alpha$-Sn | 13.1 | -5.9 | 30.5 |
| oP12-$NaSn_3$ | aP76-$Na_7Sn_{12}$ ↔ $\alpha$-Sn | 15.1 | -6.0 | 36.7 |
| oI12-$NaSn_5$* | mS48-$NaSn_2$ ↔ $\alpha$-Sn | 31.3 | 11.0 | 77.2 |
| oI12-$NaSn_5$* | aP76-$Na_7Sn_{12}$ ↔ $\alpha$-Sn | 32.6 | 10.9 | 81.4 |
| tP12-$NaSn_5$ | mS48-$NaSn_2$ ↔ $\alpha$-Sn | 6.3 | -3.2 | -0.5 |
| tP12-$NaSn_5$ | aP76-$Na_7Sn_{12}$ ↔ $\alpha$-Sn | 7.7 | -3.3 | 3.7 |

Supplementary Table 1. Energy differences for select Na-Sn phases with respect to relevant polymorphs or tie-lines at ambient pressure and zero temperature evaluated with three DFT approximations. All structures were fully (re)optimized with each DFT flavor. Thermodynamically stable and other important phases found in our searches are marked with asterisks and daggers, respectively.

| Phase | Relative to | PBE | LDA | SCAN |
|---|---|---|---|---|
| cP4-$Ca_3Sn$ | fcc-Ca ↔ oP12-$Ca_2Sn$ | 40.4 | 21.7 | 51.8 |
| hP6-$Ca_2Sn$† | oP12-$Ca_2Sn$ | 9.0 | -4.3 | 8.6 |
| oP12-$Ca_2Sn$† | oP12-$Ca_2Sn$ | 2.4 | -3.8 | 3.5 |
| oS16-$Ca_5Sn_3$ | oP12-$Ca_2Sn$ ↔ tI204-$Ca_{31}Sn_{20}$ | 108.0 | - | - |
| tI32-$Ca_5Sn_3$ | oP12-$Ca_2Sn$ ↔ tI204-$Ca_{31}Sn_{20}$ | 7.8 | - | - |
| tP118-$Ca_{36}Sn_{23}$ | oP12-$Ca_2Sn$ ↔ tI204-$Ca_{31}Sn_{20}$ | 2.3 | - | - |
| oP52-$Ca_7Sn_6$ | tI204-$Ca_{31}Sn_{20}$ ↔ oS8-CaSn | 8.8 | - | - |
| tP2-CaSn | oS8-CaSn | 31.6 | 16.3 | 39.3 |
| oS16-CaSn† | oS8-CaSn | 5.7 | 5.1 | 5.6 |
| oS32-$Ca_3Sn_5$† | oS8-CaSn ↔ cP4-$CaSn_3$ | 6.3 | 1.4 | -8.5 |
| hR9-$CaSn_2$† | oS8-CaSn ↔ cP4-$CaSn_3$ | 7.5 | 30.6 | -16.5 |

Supplementary Table 2. Energy differences for select Ca-Sn phases with respect to relevant polymorphs or tie-lines at ambient pressure and zero temperature evaluated with three DFT approximations. All structures were fully (re)optimized with each DFT flavor. Thermodynamically stable and other important phases found in our searches are marked with asterisks and daggers, respectively.

| Phase | Relative to | PBE | LDA | SCAN |
|---|---|---|---|---|
| hP26-$Cu_{10}Sn_3$ | fcc-Cu ↔ hP4-CuSn | 21.5 | 25.6 | 34.4 |
| oP8-$Cu_3Sn$ | fcc-Cu ↔ hP4-CuSn | 17.4 | 22.9 | 36.0 |
| hP8-$Cu_3Sn$ | fcc-Cu ↔ hP4-CuSn | 14.9 | 20.0 | 32.9 |
| cF16-$Cu_3Sn$ | fcc-Cu ↔ hP4-CuSn | 75.5 | 89.3 | 98.7 |
| hP8-$Cu_3Sn$ | fcc-Cu ↔ hP4-CuSn | 14.9 | 20.0 | 32.3 |
| oS80-$Cu_3Sn$ | fcc-Cu ↔ hP4-CuSn | 15.9 | 21.3 | 33.9 |
| tI12-$Cu_2Sn$† | fcc-Cu ↔ hP4-CuSn | 8.1 | 8.5 | 24.6 |
| mS54-$Cu_5Sn_4$ | fcc-Cu ↔ hP4-CuSn | 10.0 | 16.4 | - |
| mP36-$Cu_5Sn_4$ | fcc-Cu ↔ hP4-CuSn | 7.1 | 13.0 | 17.2 |
| mS44-$Cu_6Sn_5$ | fcc-Cu ↔ hP4-CuSn | 4.8 | 9.3 | 11.1 |
| oS20-$CuSn_4$ | hP4-CuSn ↔ $\alpha$-Sn | 38.7 | 30.3 | - |
| tP10-$CuSn_4$* | hP4-CuSn ↔ $\alpha$-Sn | 37.4 | 31.9 | - |

Supplementary Table 3. Energy differences for select Cu-Sn phases with respect to relevant polymorphs or tie-lines at ambient pressure and zero temperature evaluated with three DFT approximations. All structures were fully (re)optimized with each DFT flavor. Thermodynamically stable and other important phases found in our searches are marked with asterisks and daggers, respectively.

| Phase | Relative to | PBE | LDA | SCAN |
|---|---|---|---|---|
| aP9-$Pd_8Sn$* | fcc-Pd ↔ cP4-$Pd_3Sn$ | -23.2 | -21.2 | -27.5 |
| tI18-$Pd_8Sn$ | fcc-Pd ↔ cP4-$Pd_3Sn$ | -21.3 | -20.1 | -26.2 |
| tI18-$Pd_8Sn$ | aP9-$Pd_8Sn$* | 1.9 | 1.1 | 1.3 |
| aP8-$Pd_7Sn$† | fcc-Pd ↔ cP4-$Pd_3Sn$ | -24.3 | -22.1 | -29.1 |
| aP8-$Pd_7Sn$† | aP9-$Pd_8Sn$* ↔ hR21-$Pd_6Sn$* | 0.6 | 0.6 | 0.9 |
| hR21-$Pd_6Sn$* | fcc-Pd ↔ cP4-$Pd_3Sn$ | -27.0 | -24.6 | -33.2 |
| mS12-$Pd_5Sn$ | fcc-Pd ↔ cP4-$Pd_3Sn$ | -14.0 | -10.9 | -19.6 |
| mS12-$Pd_5Sn$* | fcc-Pd ↔ cP4-$Pd_3Sn$ | -22.2 | -20.1 | -30.1 |
| mS12-$Pd_5Sn$ | mS12-$Pd_5Sn$* | 8.1 | 9.1 | 10.5 |
| mS32-$Pd_5Sn_3$* | oP12-$Pd_2Sn$ ↔ oP8-PdSn | -1.8 | -3.0 | -3.4 |
| tI36-$PdSn_2$* | tI48-$PdSn_2$ | -1.3 | 0.8 | -10.6 |
| oS32-$PdSn_3$ | tI48-$PdSn_2$ ↔ oS20-$PdSn_4$ | 4.4 | 3.8 | 20.6 |
| oS32-$PdSn_3$ | tI36-$PdSn_2$* ↔ oS20-$PdSn_4$ | 4.9 | 3.5 | 24.6 |

Supplementary Table 4. Energy differences for select Pd-Sn phases with respect to relevant polymorphs or tie-lines at ambient pressure and zero temperature evaluated with three DFT approximations. All structures were fully (re)optimized with each DFT flavor. Thermodynamically stable and other important phases found in our searches are marked with asterisks and daggers, respectively.

| Phase | Relative to | PBE | LDA | SCAN |
|---|---|---|---|---|
| hP8-$Ag_7Sn$† | fcc-Ag ↔ oP8-$Ag_3Sn$ | 0.2 | -1.1 | 0.7 |
| mP16-$Ag_7Sn$† | fcc-Ag ↔ oP8-$Ag_3Sn$ | 0.4 | -1.8 | 1.2 |
| mP14-$Ag_6Sn$† | fcc-Ag ↔ oP8-$Ag_3Sn$ | 0.7 | -1.5 | 2.4 |
| hR21-$Ag_6Sn$† | fcc-Ag ↔ oP8-$Ag_3Sn$ | 2.6 | 2.0 | 3.6 |
| mP12-$Ag_5Sn$† | fcc-Ag ↔ oP8-$Ag_3Sn$ | 1.1 | -0.7 | 2.1 |
| mS44-$Ag_9Sn_2$† | fcc-Ag ↔ oP8-$Ag_3Sn$ | 1.9 | 0.4 | 3.5 |
| mP16-$Ag_{13}Sn_3$† | fcc-Ag ↔ oP8-$Ag_3Sn$ | 1.7 | -0.2 | 3.8 |
| mP10-$Ag_4Sn$† | fcc-Ag ↔ oP8-$Ag_3Sn$ | 0.3 | -1.4 | 1.7 |
| mP18-$Ag_7Sn_2$† | fcc-Ag ↔ oP8-$Ag_3Sn$ | 0.2 | -0.7 | 1.5 |
| tI12-$AgSn_2$* | oP8-$Ag_3Sn$ ↔ $\alpha$-Sn | 28.9 | 17.4 | - |
| tI10-$AgSn_4$* | oP8-$Ag_3Sn$ ↔ $\alpha$-Sn | 60.4 | 53.7 | - |

Supplementary Table 5. Energy differences for select Ag-Sn phases with respect to relevant polymorphs or tie-lines at ambient pressure and zero temperature evaluated with three DFT approximations. All structures were fully (re)optimized with each DFT flavor. Thermodynamically stable and other important phases found in our searches are marked with asterisks and daggers, respectively.

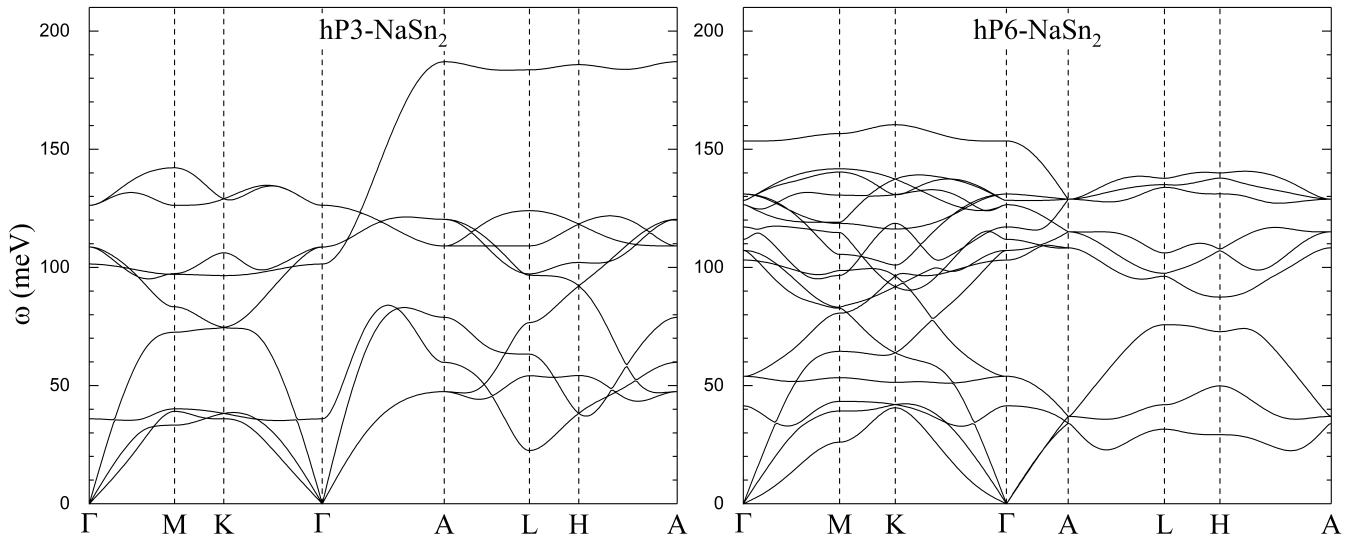


Supplementary Figure 7. Phonon dispersions for hP3-$NaSn_2$ and hP6-$NaSn_2$ phases calculated at the PBE level with the finite displacement method. The hP3-$NaSn_2$ (hP6-$NaSn_2$) phase was calculated with a $3 \times 3 \times 4$ ($3 \times 3 \times 2$) expansion of the conventional unit cell. Displacements for both phases were calculated with a $4 \times 4 \times 4$ k-mesh centered on the Γ-point. The results indicate that both phases are dynamically stable and that the distortion of the honeycomb Sn framework leading to the doubling of the unit cell softens the highest optical modes.

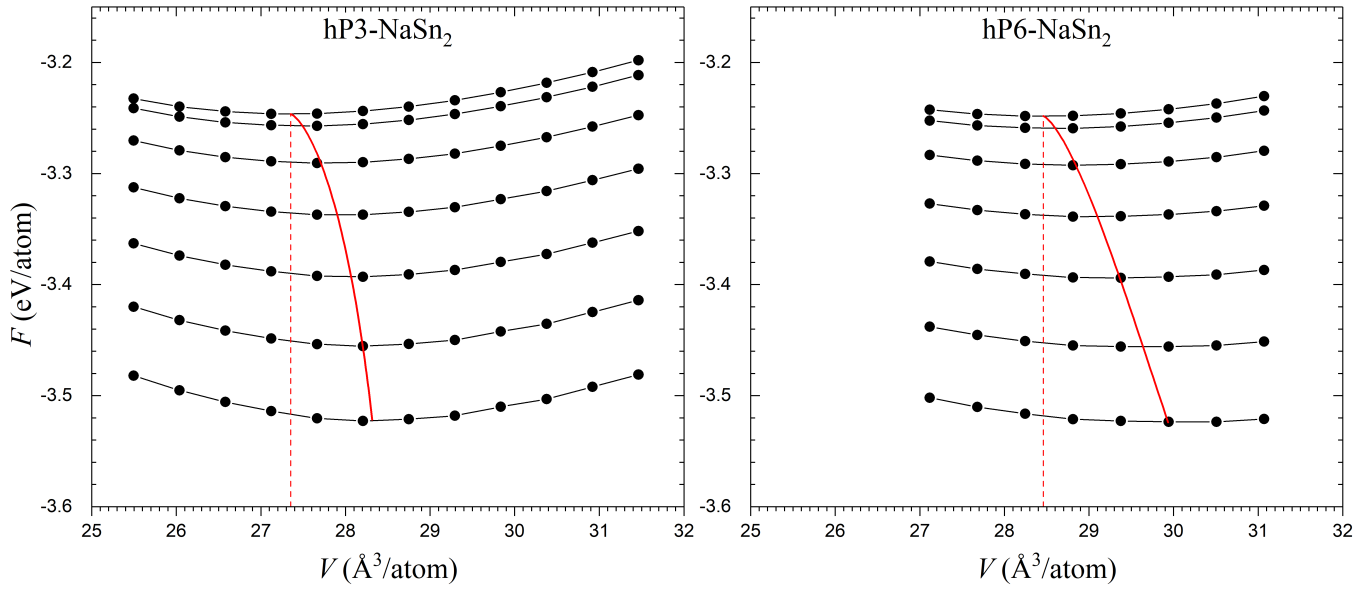


Supplementary Figure 8. Quasi-harmonic (QH) results for hP3-$NaSn_2$ and hP6-$NaSn_2$. In these simulations, we (i) generated a uniform grid of volumes around equilibrium by rescaling the lattice constants; (ii) optimized the unit cell shape and atomic positions at each fixed volume with VASP; (iii) used Phonopy and VASP to perform phonon calculations in the harmonic approximation at each volume; (iv) fitted the resulting free energy points at each temperature with a third-order polynomial; and (v) showed the free energy values for every 100 K from 0 K to 600 K (black circles), the polynomial fits (black solid lines), the minimum free energy values at the corresponding volumes for every 10 K (red solid line), and the starting volume (red dashed line).

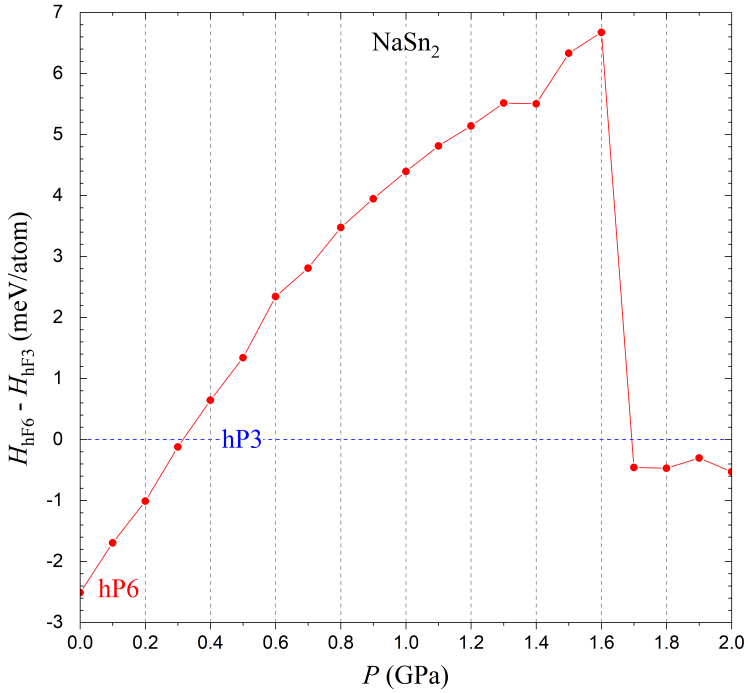


Supplementary Figure 9. Relative enthalpy of hP6-$NaSn_2$ with respect to hP3-$NaSn_2$ as a function of hydrostatic pressure. At each pressure, both structures were fully relaxed starting from their ambient-pressure optimized unit cells. The hP6 minimum becomes unfavorable above 0.4 GPa and disappears above 1.7 GPa.

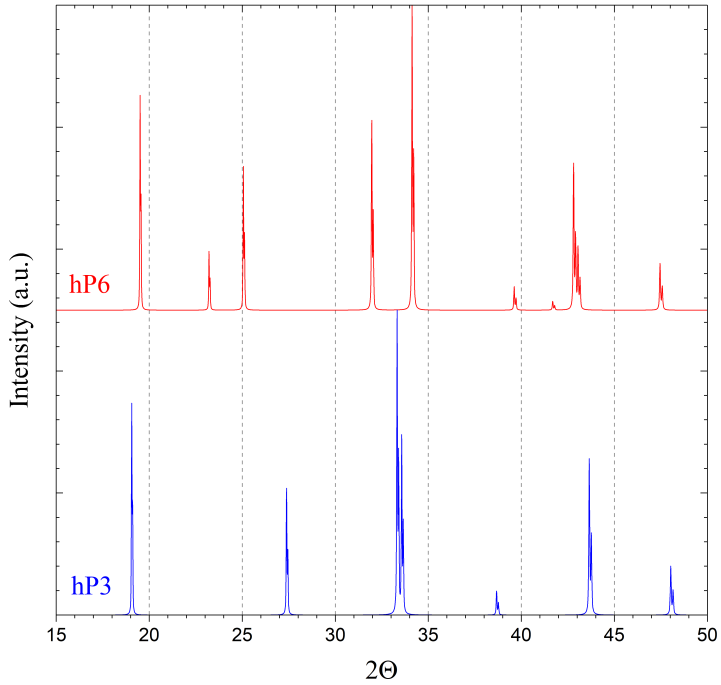


Supplementary Figure 10. Simulated powder x-ray diffraction (XRD) patterns for two related hP3 and hP6 phases of $NaSn_2$. The distortion of the Sn honeycomb framework results in the doubling of the unit cell and a considerable difference in the position of the XRD peaks.

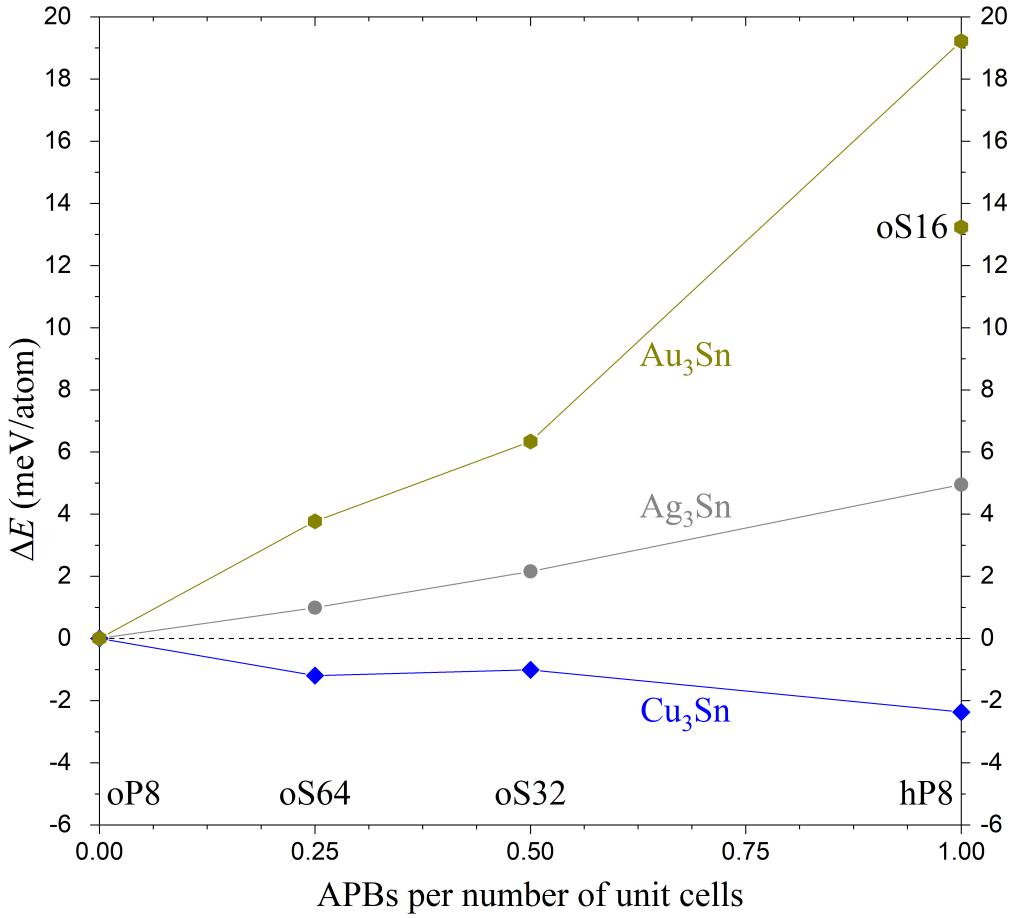


Supplementary Figure 11. Relative stability of $M_3Sn$ phases (M = Cu, Ag, Au) with a different number of anti-phase boundaries (APBs). The oP8 structure with the $Cu_3Ti$ prototype has no APBs. The structure with the maximum number of APBs and can be represented with a hexagonal hP8 unit cell. The relaxation of the hP8-$Au_3Sn$ phase in the orthorhombic oS16 representation resulted in a noticeable relative energy drop from 19 meV/atom to 13 meV/atom due to symmetry breaking.